Chemical Engineering Journal 505 (2025) 159761

Contents lists available at ScienceDirect

Chemical Engineering Journal

journal homepage: www.elsevier.com/locate/cej

Ultrafast preparations of metal magnesium by Joule-heating vacuum carbothermal reduction

Xiao Luo, Peng Zhao *, Jiangjiang Li

School of Materials Science & Engineering, Chang'an University, Xi'an, 710061, Shaanxi, PR China

ARTICLE INFO

Keywords:
Magnesium
Joule-heating
Vacuum carbothermal reduction
Reduction mechanism
Condensation

ABSTRACT

The traditional vacuum carbothermal reduction (VCTR) process is severely hampered by sluggish processing kinetics, typically reaction time of several hours, which is time and energy consuming. Additionally, the obtained magnesium powder poses a significant risk of explosion. Here a Joule-heating vacuum carbothermal reduction (JHVCTR) process is developed for the preparation of bulk magnesium with uniform temperature profiles, rapid heating/cooling, and short reaction times. MgO in CaO·MgO-C pellets can be reduced by the JHVCTR process within 120 s with a reduction rate of 95.83 %. The kinetic analysis demonstrates that the reaction between MgO and C is dominated by the phase boundary reaction, and the activation energy is 169.1 kJ•mol^{-1}. Theoretical analysis based on Joule's law indicates that Joule heating can form an extremely high-temperature C-MgO interface, which facilitates the processing reactions. Meanwhile, molecular dynamics (MD) simulations and density functional theory (DFT) calculations demonstrate that the applied electric field during the JHVCTR process can reduce the binding ability of MgO, thereby enhancing its reactivity and facilitating the reaction rate. Then, the resulted magnesium vapor is successfully condensed into a compact magnesium bulk with high purity at 647 °C. Thermodynamic analysis confirms that high condensation temperatures can mitigate the inverse reaction between magnesium vapor and CO. Besides, the scale-up trials are also conducted to explore the feasibility of the JHVCTR process for the industrial production of magnesium. Overall, the JHVCTR process potentially provides a rapid and safe approach for the production of magnesium.

1. Introduction

Magnesium is a critical alkaline earth metal with enormous reserves. Magnesium and its alloys are extensively used in the aerospace, vehicle, desulfurization, metallurgy, solid-state hydrogen storage, and biomedical [1–4] due to their excellent physical and chemical properties, such as low structural density, high specific strength, good biocompatibility, and recyclable features [5]. In recent years, the market demand for magnesium has been increasing dramatically at 10 % annual increments [6]. Meanwhile, the price of magnesium, which in the past few years fluctuated around \$2000 ton^{-1}, skyrocketed to more than \$11,000 ton^{-1} in September 2021 [7]. This stimulates the commercial developments for the production of magnesium.

Currently, the common routes for commercially preparing magnesium include thermal reduction and electrolysis. Among them, the Pidgeon process (silicon thermal reduction) is the dominant contributor because of its small capital cost and low technical threshold, which has produced approximately 85 % of the global primary magnesium in China [8]. However, the Pidgeon process features energy intensive and carbon intensive, with the energy consumption and carbon footprint up to 162–288 MJ and 26–42 kg CO_2 equivalent (CO_2e) per kg of magnesium produced [9]. Particularly, the adopted ferrosilicon alloy reductive agent is not only expensive but also the preparation process has substantial environmental concerns. Therefore, the magnesium industry is trying to transition to cleaner production under the restrictions of tighter environmental policy to realize carbon neutral in China.

Over the past decades, the vacuum carbothermal reduction (VCTR) process (MgO + C = Mg + CO) has attracted extensive attention for its excellent potential to save energy, reduce costs, minimize byproducts, and reduce carbon dioxide emissions. The VCTR process typically produces magnesium through the thermal reduction of calcined dolomite (CaO·MgO) or calcined magnesite (MgO), reacting with cheap carbonaceous reductant (such as charcoal, activated carbon, and coke) under vacuum. Compared to the Pidgeon process, the VCTR process results in 63.14 %, 69.16 %, 66.67 %, and 90.45 % lower in consumption of resources and energy, greenhouse gas (GHG) emissions, and solid waste

* Corresponding author.
E-mail address: 963043279@qq.com (P. Zhao).

https://doi.org/10.1016/j.cej.2025.159761
Received 11 October 2024; Received in revised form 24 December 2024; Accepted 19 January 2025
Available online 20 January 2025

generation, respectively [10]. So far, many investigators explored the physicochemical fundamentals involving the process mechanism [11], thermodynamics [12], and kinetics [13] of the VCTR reaction, the catalytic behavior of CaF_2 [14], the mechanism of reverse reaction [15] and the condensation laws of magnesium vapor [16] to improve reduction efficiency and quality of the product. Nevertheless, some drawbacks in the VCTR process still need to be overcome. First, VCTR is a thermally driven solid–solid reaction [17], which was controlled by sluggish mass transfer of the C atoms and MgO. Hence, to obtain a high reduction rate of MgO, the heating duration of VCTR reaction with hours (1–4 h) at 1350–1500 °C is necessary [18], which typically results in high energy and time consumption. Moreover, hours at a high temperature can easily lead to serious sintering of MgO particles, consequently causing a decrease in the reaction activity of MgO and a loss of contact between MgO and C [19,20], thereby hindering the reduction of MgO. Besides, the inverse reaction between produced magnesium vapor and CO (Mg + CO = MgO + C) in the condensation process is an inevitable bottleneck, destroying the quality of the product. Extensive efforts to overcome the critical problem include condensing within a cold gas, into hydrocarbon oils, and onto solid particles [21], as well as supersonic quenching using Laval nozzle [22]. However, all of these technologies lead to a vital issue of generating fine powders through ultra-fast nucleation and growth, which has the potential risk of self-ignition or even explosion [23]. Therefore, a new technique is urgently required for the rapid preparation of magnesium and the effective condensation of magnesium vapor in the VCTR process.

Recently, Joule-heating technology has emerged as a hot research topic due to its high efficiency and rapidity, that has been extended in a range of materials preparation and metallurgical process [24,25], including for the evaporative separation of metals from electronic waste [26], the heavy metal removal from coal fly ash for low-carbon footprint cement [27], the electrothermal chlorination separation of individual critical metals from electronic waste [28], and even the cleaner calcination of dolomite for magnesium production through carbothermal reduction [29].

In this work, we for the first time reported the rapid preparation of bulk magnesium by Joule-heating vacuum carbothermal reduction (JHVCTR) process. Fig. 1 shows the schematic illustration of the preparation process of magnesium by JHVCTR and traditional VCTR. In the traditional VCTR process, the sample is slowly heated by thermal radiation in an electric furnace. Due to the sluggish processing kinetics, the reduction period usually proceeds with hours. Then, the produced magnesium vapor is rapidly quenched and obtains fine magnesium powder. In our proposed JHVCR process, an in-situ Joule-heating technique was developed to drive the vacuum carbothermal reduction reaction of MgO, which can instantaneously heat the sample to high temperatures. Due to kinetics-dominated characteristics, the reduction process can be completed within 120 s, which constrains the sintering of MgO particles, increasing the reduction rate of MgO, and, more importantly, potentially reducing the energy consumption compared with traditional VCTR process. Meanwhile, the produced magnesium vapor is vacuum deposited onto a radiation-heated condenser and well-crystallized bulk magnesium is obtained. Herein, the JHVCTR process is systematically studied. The optimum reaction parameters (input power density and reaction time) and condensation temperature are determined. Moreover, the reaction mechanism of JHVCTR and the vacuum condensation are revealed. Furthermore, the potential scalability of the JHVCTR process for the production of magnesium is investigated in the laboratory. In summary, our research provides a promising strategy for rapid, efficient, and high-quality preparation of bulk magnesium.

2. Experimental section

2.1. Materials

Calcined dolomite (CaO·MgO), semi-coke, and fluorite were obtained from the Yulin TianLong magnesium Co. LTD. The relative content of each chemical composition is shown in Table 1. Graphite (purity, >98 %) was bought from Tianjin Zhiyuan Chemical Reagent Co., Ltd.

2.2. Magnesium production via the JHVCTR process

For the production of magnesium, calcined dolomite and semi-coke were used as magnesium resource and reductant, respectively. They were ground into powder with a particle <50 μm. Graphite with a particle size of 4–8 μm worked here as a conductive additive. Fluorite with a particle size of 10–15 μm was used as the catalyst. First, calcined dolomite powder, semi-coke powder (in a C/MgO molar ratio of 1.5), graphite (5 wt%), and fluorite (5 wt%) were evenly mixed by using a ball mill (XQM-0.4A) for 1 h. Then, 0.42 g of the mixture was pressed to form a CaO·MgO-C pellet (6 mm in diameter and 8 mm in height) under 15 MPa. Next, the pellet was placed into the homemade JHVCR device (as Fig. 2a), linked by two graphite electrodes with an alternating-current source, and then rapidly heated (in about 1–2 s) to the set temperature (1250–1450 °C, determined in real time by a PT-300B infrared thermometer and altered by precisely regulating the input power density) for 30–180 s in 10 Pa to carry out the reduction reaction between MgO and C. After the reaction, the pellet was quickly quenched (in about

Table 1
The relative content of each chemical composition in calcined dolomite, semi-coke, and fluorite (wt.%).

Calcined dolomite	CaO	MgO	SiO_2	Al_2O_3	Fe_2O_3
	56.31	42.15	0.84	0.22	0.15
Semi-coke	Fixed carbon	Ash	Sulfuric	Volatile component	
	75.77	19.88	2.33	2.02	
Fluorite	CaF_2	P	SiO_2	S	Fe_2O_3
	95.04	0.22	1.11	0.62	2.22

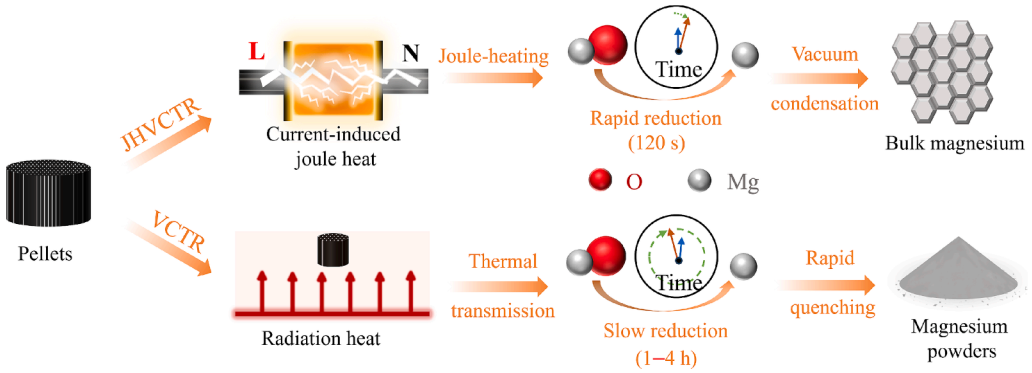

Fig. 1. Schematic illustration of the preparation process of magnesium by JHVCTR process and traditional VCTR process.

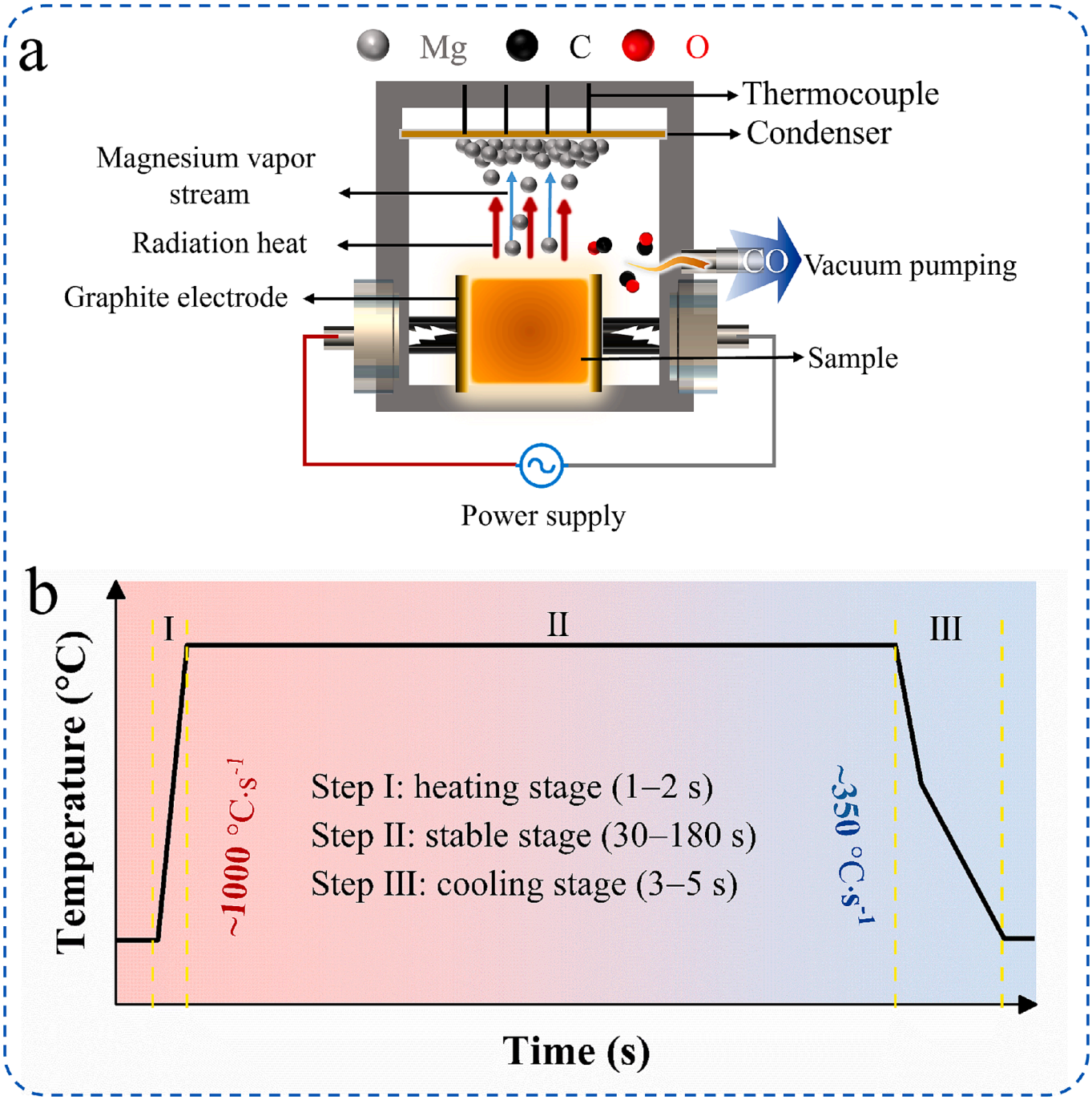

Fig. 2. (a) The schematic of the JHVCTR device. (b) Temporal evolution of temperature during the Joule-heating.

3–5 s) to room temperature triggered by turning off the power. As shown in Fig. 2b, the average heating and cooling rate of Joule-heating approached 1000 and 350 °C·s^{-1}, respectively. Finally, the volatile magnesium vapors were deposited onto a condenser (alumina ceramic plate: 50 × 20 × 1 mm, heated by thermal radiation of hot CaO·MgO-C pellet, and the temperature of the condenser was controlled by regulating the distance between the condenser and heated CaO·MgO-C pellet) to obtain the magnesium product. An example of a residual CaO·MgO-C pellet code is RP-58. The RP denotes the acronym of residual pellet, and 58 denotes the reduction rate of MgO (molar percentage) in CaO·MgO-C pellet.

2.3. Reduction rate analysis and characterizations

The reduction rate of MgO in CaO·MgO-C pellets was calculated according to Eq. (1).

$$\alpha_r = \frac{m_b - m_a}{m_b} \tag{1}$$

where α_r (wt%) denotes the reduction rate of MgO; m_b and m_a denotes the mass of MgO in CaO·MgO-C pellets before and after reduction.

The crystalline structure and surface morphology of the raw CaO·MgO-C pellets, residual CaO·MgO-C pellets, and obtained magnesium product were investigated by scanning electron microscope (SEM, Hitachi S-4800) and powder X-ray diffractometer (XRD, Bruker D8

Advance, Cu Kα radiation, λ = 1.54 Å, 0.02°·s^{-1}), respectively. The average crystalline sizes of MgO and CaO in CaO·MgO-C pellets before and after the JHVCTR process were calculated by using the Scherrer formula (Eq. (2)).

$$D_a = \frac{k\lambda}{\beta cos\theta} \quad (2)$$

where D_a (nm) denotes the average size of crystallite; k (0.89) denotes the Scherrer constant; λ (nm) denotes the wavelength of the scanned X-ray; β denotes the full width at half maximum (FWHM) of the diffraction peak, and θ (∘) denotes the Bragg angle of the diffraction peaks.

The Quantitative analysis of obtained magnesium products was conducted by energy-dispersive spectroscopy (EDS).

2.4. Simulations of temperature distribution during Joule-heating

Finite element (FE) simulations were carried out using COMSOL Multiphysics 5.6 to study the steady-state temperature distribution of CaO·MgO-C pellets during Joule-heating under the different input power density (0.3, 0.35, 0.4, 0.45, 0.5 and 0.55 W·mm^{-3}). The electric conductivity, thermal conductivity, and density of CaO·MgO-C pellets were set as 40 S·m^{-1}, 120 × (300/T)·W·(m^{-1}·K^{-1}), and 1.86 g·cm^{-3}, respectively.

2.5. Kinetics studies

Kinetics studies of the reaction between MgO and C during the JHVCTR process were carried out using Eqs. (3)–(5).

$$\frac{d\alpha_r}{dt} = k_r f(\alpha_r) \quad (3)$$

$$g(\alpha_r) = k_r t \quad (4)$$

$$k_r = Aexp(\frac{E_a}{RT}) \quad (5)$$

where α_r denotes the reduction rate of MgO; t (s) denotes the reaction time; k_r (s^{-1}) denotes the reduction rate constant; $f(\alpha_r)$ denotes the reaction kinetics model; $g(\alpha_r)$ denotes the definite integral function of the reaction kinetics model $f(\alpha)$; E_a (J•mol^{-1}) denotes the activation energy; A (s^{-1}) denotes the frequency factor; R (8.314 J•mol^{-1}•K^{-1}) denotes the gas constant, and T (K) denotes the thermodynamic temperature.

2.6. Molecular dynamics simulations and first-principles density functional theory calculations

The effect of the applied electrical field on MgO reduction during the JHVCTR process was probed by the molecular dynamics (MD) simulations and the first-principles density functional theory (DFT) calculations using the Cambridge Sequential Total Energy Package (CASTEP) embedded in Material Studio.

In order to verify the interaction between MgO and C with and without an applied electrical field, a structure model of C on MgO (100) (Fig. 3a) was constructed for the MD simulations. In the simulations, a dynamic relaxation of the whole system was carried out under an NPT ensemble with a duration of 1 ps and a time step of 1 fs. The Nose thermostat and the Andersen method were collected to control the temperature at 1492 °C and the pressure at 10 Pa. The applied electrical field was in the z-axis direction.

To obtain the change of the electron density, bandgap, density of states (DOS), and the system energy of MgO under the different applied electric fields, the first-principles DFT calculations were carried out with the crystal structure model of MgO (presented in Fig. 3b). For all first-principles DFT calculations, the ultrasoft pseudopotential method was employed with the cutoff energy of 340 eV. The generalized gradient approximation (GGA) method based on the Perdew-Burke-Ernzerhof (PBE) functional was used to treat the exchange–correlation interaction. A k-point mesh of 8 × 8 × 8 was used. The convergence tolerance of energy, the maximum interatomic force, and the maximum displacement were set at 1.0 × 10^{-5} eV/atom, 0.5 eV/atom, and 1.0 × 10^{-3} Å, respectively.

3. Results and discussions

3.1. Rapid reduction of MgO with the JHVCTR process

3.1.1. Optimizing JHVCTR parameters

In the JHVCTR process, the temperature of the CaO·MgO-C pellets was precisely altered by regulating the input power density (0.3 to 0.55 W·mm^{-3}). As shown in Fig. 4a, the average temperature of CaO·MgO-C pellets increased as the input power density increased, and could reach as high as 1492 °C at 0.55 W·mm^{-3}. The FE simulations confirmed that

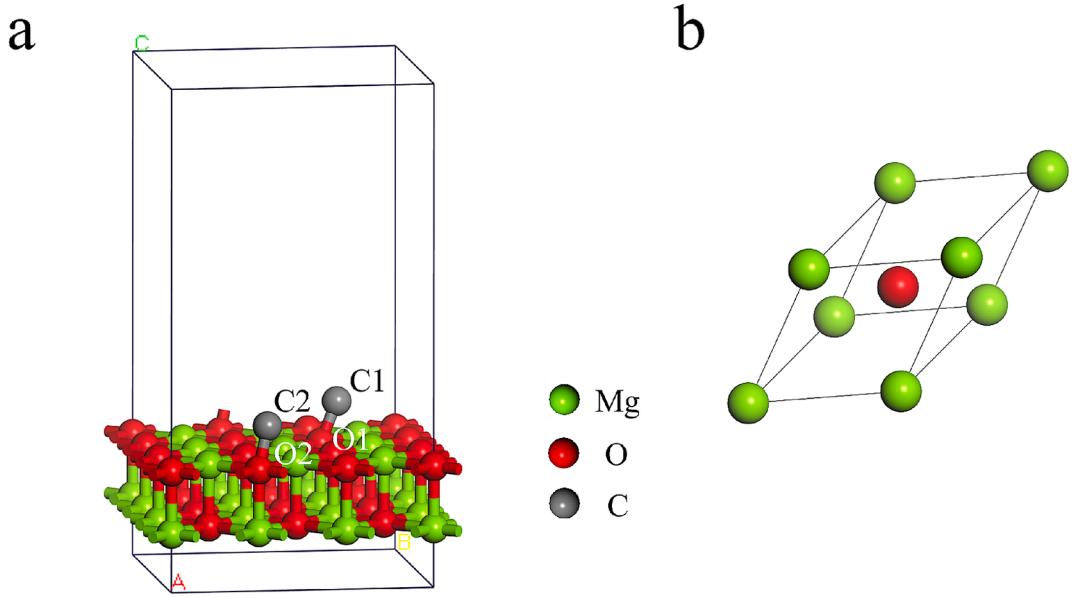

Fig. 3. (a) The crystal structure model of MgO. (b) The structure model of C on MgO (100).

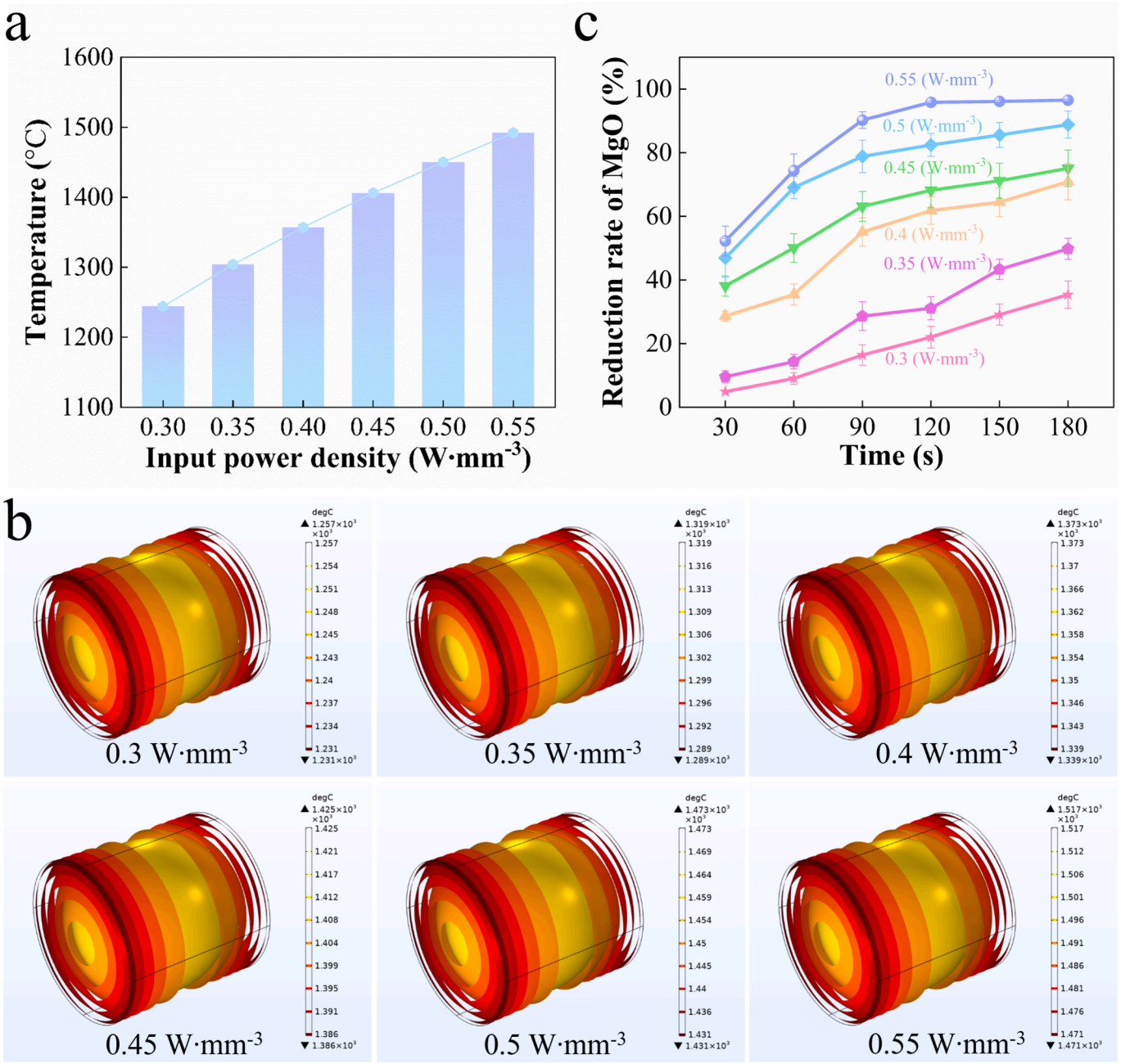

Fig. 4. (a) The average temperature and (b) the temperature distribution of the CaO·MgO-C pellets during the JHVCR process under various input power densities. (c) The reduction rate of MgO in CaO·MgO-C pellets under different input power densities and reaction times.

Joule-heating could form a relatively homogeneous temperature distribution (Fig. 4b), which guaranteed the uniform thermal effect on CaO·MgO-C pellets. In order to screen the optimum JHVCTR reaction parameters, the effect of input power density and reaction time on the MgO reduction reaction with the JHVCTR process was explored (Fig. 4c). With a fixed reaction time, the reduction rate of MgO increased with input power density constantly. Meanwhile, extending the reaction time at a constant input power density led to a similar trend. It was observed that when input power density was set at 0.55 W•mm^{-3}, the reduction rate would not improve obviously when the reaction time exceeded 120 s. As a consequence, the optimum input power density and reaction time were ascertained as 0.55 W•mm^{-3} and 120 s (α_r = 95.83 %), respectively, comprehensively considering energy and time conservation as well as the high reduction rate of MgO. Notably, the reduction time of our method is more than 20 times less than the traditional VCTR process, indicating its potential for high energy-efficient preparation of magnesium.

3.1.2. *Characterizations of the residual CaO·MgO-C pellets*

XRD patterns of these residual CaO·MgO-C pellets were shown in Fig. 5. The diffraction peaks intensity of MgO gradually weakened as the input power density or reaction time increased, which verified the conversion of MgO to magnesium in the JHVCTR process. Instead, the diffraction peak intensity of CaO remained stable. The result indicated that CaO in CaO·MgO-C pellets was barely reduced even though the actual temperature had exceeded the thermodynamic critical temperature (1279 °C at 10 Pa) for CaO reduction. It could be ascribed to that carbon was preferentially utilized by MgO reduction with limited carbon supply (C/CaO·MgO < 2) [30].

To understand the reduced phenomena of the JHVCTR process, the

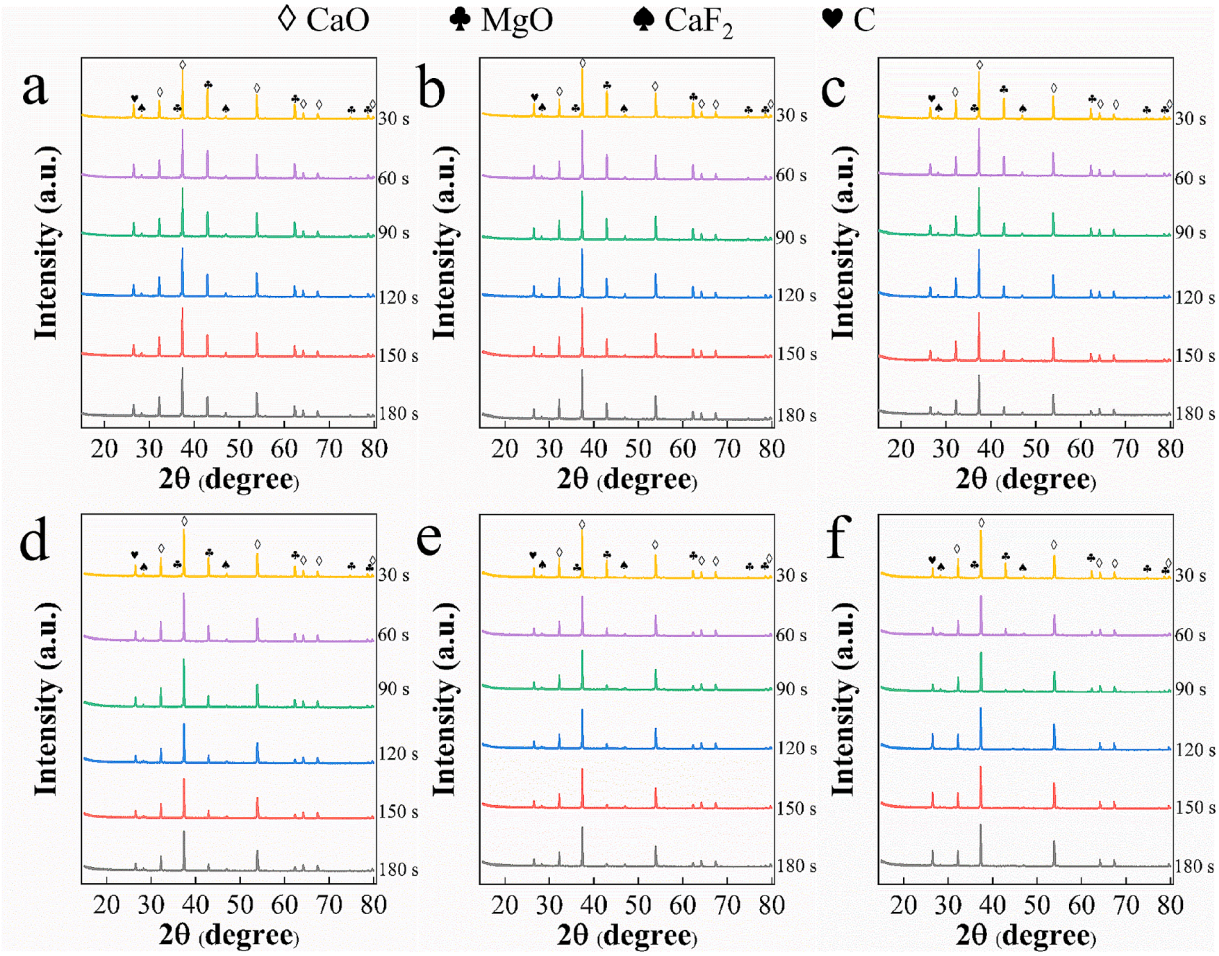

Fig. 5. XRD patterns of the residual CaO·MgO-C pellets after the JHVCTR process at an input power density (a) 0.3 W·mm^{-3}, (b) 0.35 W·mm^{-3}, (c) 0.4 W·mm^{-3}, (d) 0.45 W·mm^{-3}, (e) 0.5 W·mm^{-3}, and (f) 0.55 W·mm^{-3} with different reaction times.

average crystalline sizes of MgO and CaO (Table 2) in raw and residual CaO·MgO-C pellets were estimated by the Scherrer formula. Normally for traditional VCTR, MgO is expected to be sintered at elevated temperatures for a long-lasting duration, thus causing a decay in the reaction activity of MgO and loss of contact between MgO with C [19,20], which hinders the reduction of MgO. However, in our work, the sizes of MgO are only slightly enlarged after the JHVCTR process, owing to short reaction time and distinct thermal path (discussed in Section 3.3.1), which minimized the sintering effect on MgO reactivity and consequently increased the reduction rate of MgO. Compared to MgO, the sizes of CaO have increased significantly induced by the low Tammann temperature of CaO [31], which accelerates the sintering of CaO. Hence, a small amount of MgO surrounded by a close CaO layer is prevented from contacting with C, and thus difficult to be completely reduced.

Table 2
The average crystalline sizes of CaO and MgO in raw and residual CaO·MgO-C pellets.

Pellets	CaO (200)		MgO (200)	
	FWHM	Average size (nm)	FWHM	Average size (nm)
RP-0	0.169	49.7	0.166	50.6
RP-28.64	0.164	51.2	0.161	52.1
RP-50.07	0.161	52.1	0.158	53.1
RP-74.38	0.159	52.8	0.157	53.5
RP-95.28	0.143	58.9	—	—

"—" represents blank data, because no diffraction peak of MgO was detected in RP-95.28.

Typically, during the traditional VCTR process, the structure of reacted pellets becomes very loose due to the destruction of vigorously diffused magnesium vapor and CO, worsening the direct contact between MgO and C, and consequently leading to the increase of diffusion space of solid reactants. Hence, a longer reaction time (>1 h) was required. Herein, we observed the morphology of residual CaO·MgO-C pellets obtained at 0.55 W•mm^{-3} with different reaction times, as shown in Fig. 6. With the extension of reaction time, the volume of the residual CaO·MgO-C pellets shrunk gradually and the pores on the surface increased continually. However, it is noted that residual CaO·MgO-C pellets remain relatively dense, which guarantees good contact between MgO and C during the JHVCTR process. Therefore, the interfacial reaction of MgO and C can be carried out rapidly (120 s).

3.2. Reaction kinetic studies

In order to better understand the mechanism of MgO reduction by the JHVCTR process, the reaction kinetics were studied. According to the reports in previous literature [32], the reaction of MgO and C was mainly controlled by the phase-boundary reaction, the diffusion process of product, and the nucleation process of product, which could be represented by Eqs. (6)–(8), respectively.

For the phase-boundary reaction:

$$g(\alpha_r) = 1 - (1 - \alpha_r)^{1/3} \quad (6)$$

For the diffusion process of product:

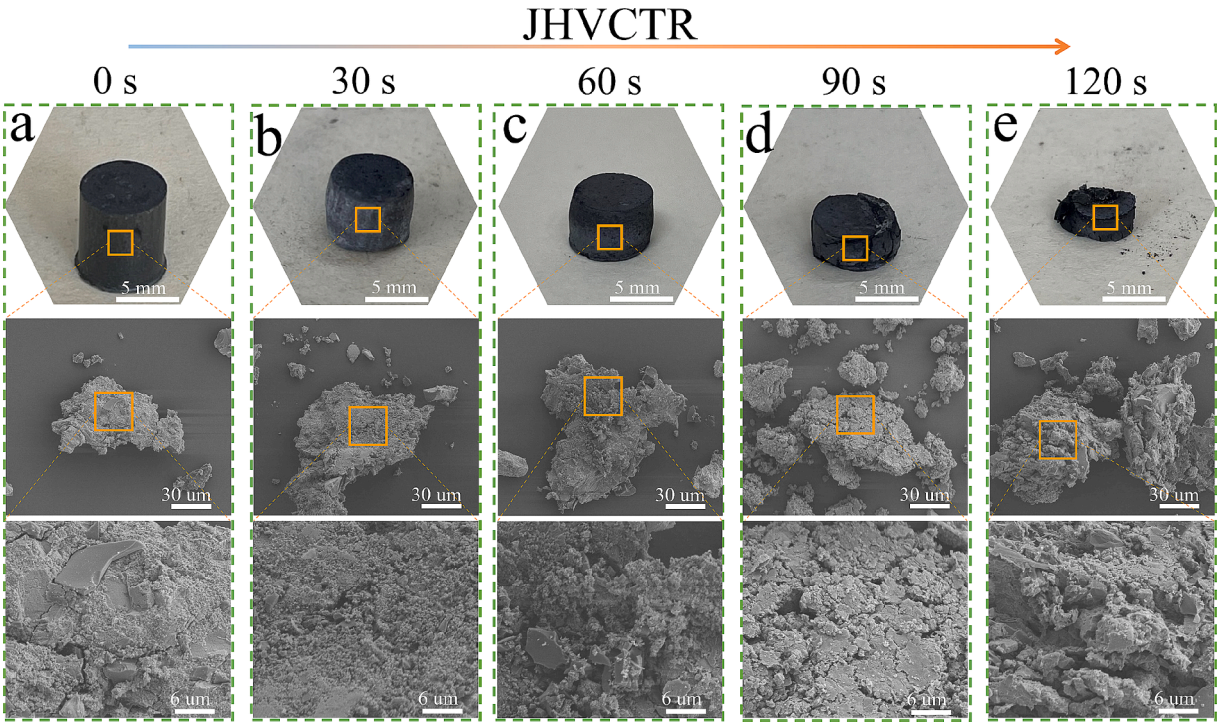

Fig. 6. Morphology of residual CaO·MgO-C pellets obtained at 0.55 W•mm^{-3} with different reaction times.

$$g(\alpha_r) = 1 - 2/3\alpha_r - (1-\alpha_r)^{2/3} \quad (7)$$

For the nucleation process of product:

$$g(\alpha_r) = ln(1/(1-\alpha_r)) \quad (8)$$

The relationship between each g(α_r) and time is shown in Fig. 7a–c. Moreover, the linear fitting curves of the relationship between lnk_r and 1/T of the phase-boundary reaction, the diffusion process of product, and the nucleation process of product were shown in Fig. 7d. It is found that the phase boundary reaction has the maximum reaction rate constant value (k_r) and best correlation coefficient (R^2 = 0.9881). Hence, the g(α_r) of phase boundary reaction could be used to accurately describe the rapid reduction reaction of MgO by the JHVCTR process. And the corresponding activation energy is 169.1 kJ·mol^{-1}, which is lower than those reported in the literature [13,20]. Notably, the value is also lower than the self-diffusion activation energy of Mg^{2+} (332

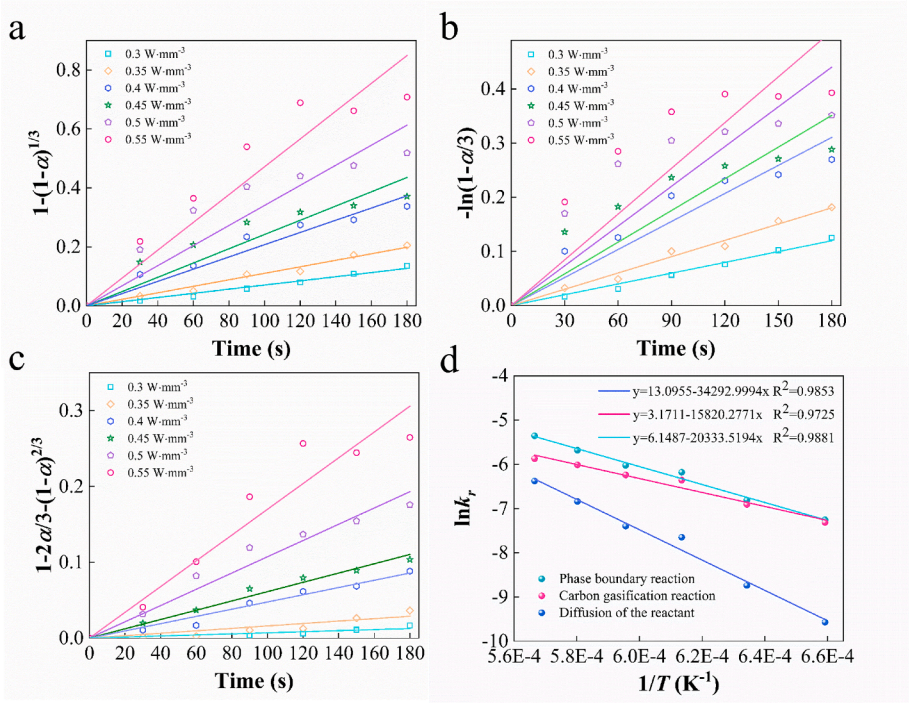

Fig. 7. The relationship between g(α_r) and time, (a) $1-(1-\alpha)^{1/3}$, (b) $-\ln(1-\alpha/3)$, (c) $1-2\alpha/3-(1-\alpha)^{2/3}$. (d) Linear fitting curves of the relationship between lnk_r and 1/T of phase-boundary reaction, diffusion process of product, and nucleation process of product.

kJ·mol^{-1}) in MgO [33], indicating that the reduction reaction of MgO in the JHVCTR process is not determined by solid-state diffusion. These results suggest that the JHVCTR process has a more positive effect on MgO reduction by decreasing the activation energy, which enhances the reaction between MgO and C.

3.3. Mechanism of enhanced reduction by JHVCTR process

3.3.1. Analysis of thermal effects induced by Joule-heating

To explain the role of the thermal effect on strengthening reduction of MgO in the JHVCTR process, we analyzed the local thermal environment in CaO·MgO-C pellets induced by Joule-heating based on Joule's law. And the schematic diagram is shown in Fig. 8. Compared to the CaO·MgO particles in the CaO·MgO-C pellet, graphite and semi-coke are more conductive and experience a larger power dissipation, producing local high-temperature hotspots [34,35]. These hotspots allow effective Joule heating and form an extremely high-temperature C-MgO interface with directly contacted CaO·MgO particles [36], which facilitates the processing reactions and accelerates the mass transfer. Meanwhile, CaO·MgO particles still maintain a relatively low interface temperature, which is helpful to mitigate the sintering behavior of MgO. Of course, the featured rapid reaction time of the JHVCTR process also is one of the key factors for small MgO crystalline sizes. Additionally, due to the high thermal conductivity of carbon, effectually triggering the thermal transformation to the whole pellet, a spatially averaged temperature distribution can be established. Hence, we believe that the local thermal environment in CaO·MgO-C pellets induced by Joule-heating is one of the reasons for facilitating the carbothermal reduction of MgO.

3.3.2. Underlying mechanism of the applied electrical field affecting MgO reduction

In this section, MD simulations were performed to explore the interaction between MgO and C with and without applied electrical field. As illustrated in Fig. 9a, under the applied electrical field-free condition (0 V·Å^{-1}), the distance of the C2-O2 bond and the C1-O1 bond reached ~1.15 Å (the bond length of CO molecule) at 240 fs and 290 fs (Fig. 9c), respectively. When the applied electrical field of 1 V·Å^{-1} is added (Fig. 9b), the same characteristics of the C2-O2 bond and the C1-O1 bond can be captured at 48 fs and 357 fs (Fig. 9d), respectively. The calculated average formation time of CO molecules with the applied electrical field (1 V·Å^{-1}) is 203 fs, which is ~31 % shorter than that without the applied electrical field (265 fs). The results indicate that the occurrence of applied electrical field plays a critical role in the rapid reduction of MgO in the JHVCTR process, which can be ascribed to the ability of applied electric fields to catalyze chemical reactions [37,38]. To our knowledge, this is the first time that the enhancement of applied electric field for carbothermal reduction of MgO was directly observed in an MD simulation.

To further validate the underlying effect of the applied electrical field on MgO reduction during the JHVCTR process, DFT calculations were performed. Fig. 10a shows the electron density of MgO under different applied electric fields. With the increase of the applied electric fields, some electrons were gradually transferred from the O atom to the Mg atom, which suggested that the interaction between the O atom and the Mg atom was weakening and the covalent bond was being disrupted between these two atoms. According to the calculated energy band structure (Fig. 10b), the increased applied electric fields result in a narrower bandgap of MgO. This leads to lower energy requirements for electron excitation, resulting in the generation of more free electrons and defects [39]. These excited electrons can be accelerated by the applied electric fields and collide with other electroneutral molecules, transmitting kinetic energy. Eventually, the diffusion flux of ions (Mg^{2+}, O^{2-}) can be increased by energetic molecules and resulting defects, which enhances the reduction of MgO [39]. Fig. 10c illustrates the DOS of MgO under varying applied electric fields. As the intensity of the applied electric field increased from 0 to 2 V·Å^{-1}, the conduction band shifted downwards towards the Fermi energy level (E_f), resulting in a narrower bandgap. This observation aligns with the aforementioned analysis of the energy band structure. Furthermore, the new orbital hybridization caused some DOS peaks to split into smaller peaks, indicating a weakening of the binding energy between the O atom and the Mg atom and making chemical bonds easier to break. In general, the energy of a compound is often used as a descriptor for its chemical stability. In this study, the system energy of MgO was calculated under various applied electric fields (Fig. 10d). The results show that the applied electric field significantly increased the system energy of MgO, leading to a decrease in its stability, which is beneficial for the reduction of MgO.

3.4. Condensation process of produced magnesium vapor

Based on previous studies [16,40], the condensation process is the key to control the quality of the magnesium products. In this part, we studied the condensation behaviors of magnesium vapor at different condensation temperatures (controlled by regulating the distance between the condenser and the heated CaO·MgO-C pellet) under an optimized reaction temperature (1492 °C) in the JHVCTR process. The relationship between the temperature of the condenser and the distance was displayed in Fig. 11a. When the distance was 5, 8, and 11 mm, the temperature of the condenser was 647, 520, and 458 °C. And the

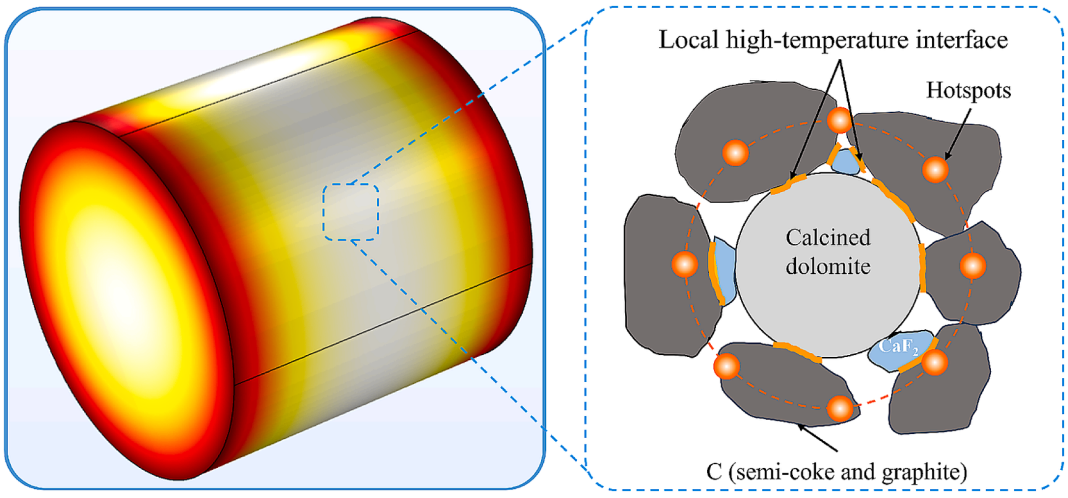

Fig. 8. Schematic of the thermal path induced by Joule-heating.

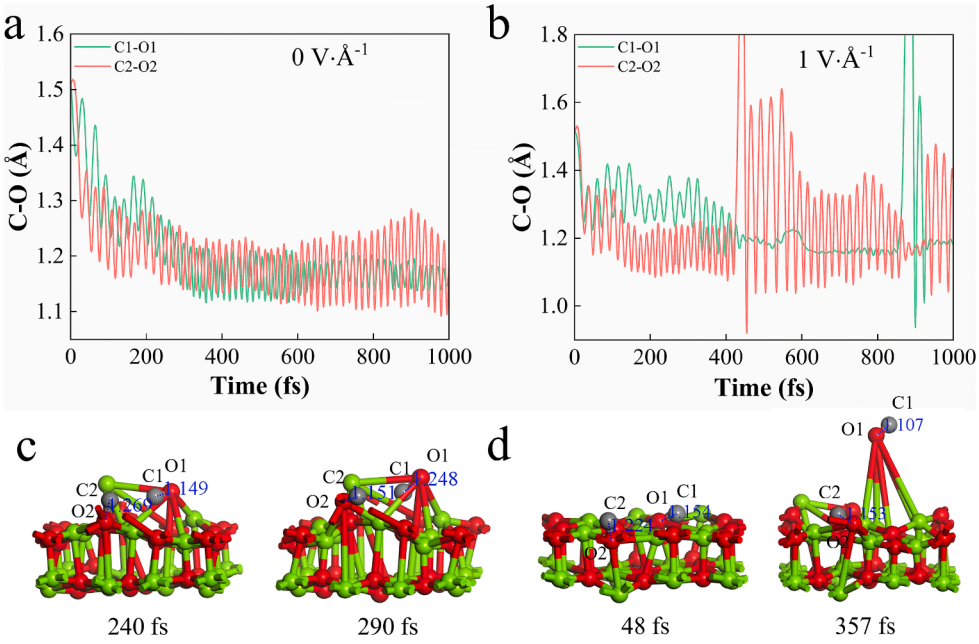

Fig. 9. (a and b) Variables of C–O distance versus simulation time (applied electric field = 0 and 1 V·Å^{-1}) at 1492 °C. (c) Simulated results of MgO (100)-C at 240 and 290 fs with an applied electric field of 0 V·Å^{-1}. (d) Simulated results of MgO (100)-C at 48 and 357 fs with an applied electric field of 1 V·Å^{-1}.

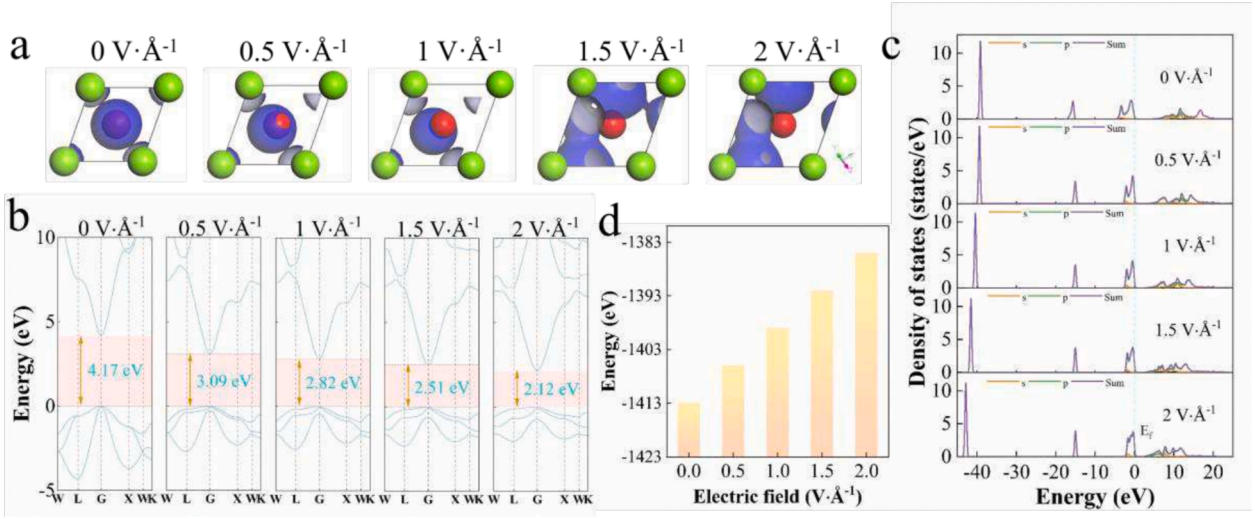

Fig. 10. The results of First-principles DFT calculations of MgO under different applied electric fields (0, 0.5, 1, 1.5, and 2 V·Å^{-1}). (a) Schematic of electron density, (b) calculated band structure, (c) total and partial DOS, and (d) the change of system energy.

corresponding products were noted as Mg-647, Mg-520, and Mg-458, respectively. The digital photographs and SEM images of these products are shown in Fig. 11b–j, which had obvious morphological differences. It is observed that as the condensation temperature decreases, the size of the products decreases apparently and the surface of the products changes gradually from dense to porous. In general, the condensation behaviors of magnesium vapor are controlled by the nucleation process and growth process. For the nucleation process, as the condensation temperature decreased, and both the critical nucleation radius of the atoms and the required nucleation atom number decreased, the nucleation of magnesium vapor benefited [41]. However, lower condensation temperature would cause magnesium vapors to nucleate simultaneously and reduce the chances of collision between Mg atoms in the growth process, thus resulting in magnesium powder [42]. Hence, it is conducive to grow dense crystal structure of magnesium by increasing the condensation temperature appropriately. Besides, the Kelvin equation [41] revealed that higher vapor pressure of magnesium was favorable for the condensation of magnesium vapor at higher condensation temperatures. Compared to the traditional VCTR process, the JHVCTR process has a shorter reaction time and higher vapor pressure of magnesium. This means that the JHVCTR process is easier to produce bulk magnesium with dense crystal structure.

To further determine the quality of these products, XRD and EDS were performed. XRD patterns (Fig. 12a) show that the diffraction peaks intensity of C and MgO increased with decreased condensation temperatures, which indicated that C and MgO contents in the obtained products were increased by decreasing the condensation temperatures. Meanwhile, quantitative EDS analysis (Fig. 12b) shows the elemental contents of C, O, and Mg in the obtained products. Mg-647 has the highest Mg content and lowest C and O contents, reaching 98.31 wt%, 0.78 wt%, and 0.91 wt%, respectively, which is coincident with XRD patterns. This phenomenon can be ascribed to the dense structure of Mg-

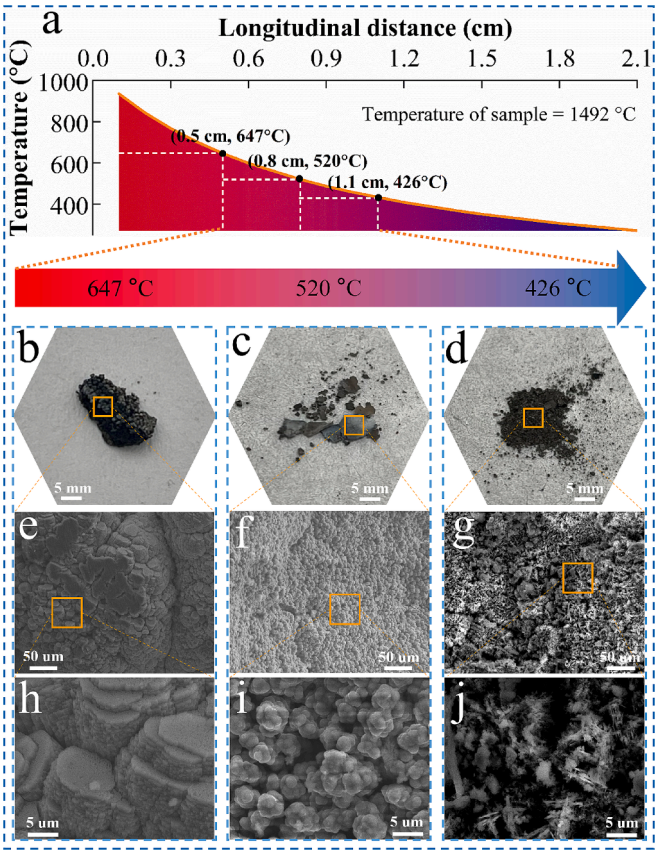

Fig. 11. (a) The longitudinal temperature profile of condenser (the temperature of the heated CaO·MgO-C pellet is 1492 °C). (b–j) Digital photographs and SEM images of Mg-647, Mg-520, and Mg-458.

647, thereby forming a low surface area, which decreases the contact with CO. Besides, the thermodynamic advantage is also an important reason. As shown in Fig. 12c, the decreased temperature is capable of reducing the value of Gibbs free energy (ΔG), suggesting that lower temperature is thermodynamically preferred for the inverse reaction. Note that the stoichiometric ratio of oxygen to carbon is close to 1:1, coinciding with the thermodynamic prediction (Fig. 12d, carried out by HSC 6.0 software), which confirms that MgO in the products has ensued from the inverse reaction (MgO + C = Mg + CO). According to the above results, the higher condensation temperature is beneficial to mitigate the inverse reaction between produced magnesium vapor and CO.

3.5. Scale-up trials

The scale-up trials of the JHVCTR process were conducted on the laboratory scale to explore its potential for industrial preparation of magnesium. Here, large-sized CaO·MgO-C pellets (3.78 g in weight, 18 mm in diameter and 8 mm in height, as the inset in Fig. S1a) were adopted. To maintain similar temperature features (temperature distribution shown in Fig. S1a, average temperature about 1492 °C), we increased the input power density (0.62 W•mm^{-3}). We were still capable of obtaining a high reduction rate of MgO (α_r = 93.04 %, Fig. S1b) after 120 s, which is comparable with the values achieved using the small-sized CaO·MgO-C pellets (α_r = 95.83 %). In addition, we traced the condensation behaviors of the produced magnesium vapor in the scale-up system. A larger size condenser (alumina ceramic plate: 100 × 30 × 1 mm) was used. The condenser is heated by thermal radiation of the hot CaO·MgO-C pellet, where the core region (560–647 °C) of the condenser has a higher temperature compared to the edge region (385–560 °C) due to its proximity to the heat source. The majority of the magnesium vapor (73.72 %) was condensed on the core region of the condenser, while the minority of the magnesium vapor (26.28 %) was condensed on the edge region of the condenser (Fig. S2). We ascribe the phenomenon to the large evaporation area of magnesium vapor and uneven temperature distribution of the condenser in the scale-up trial. The magnesium product collected from the core area has a denser structure (Fig. S3) and a higher magnesium content (Fig. S4) than that collected from the edge area. This is in agreement with the results in Section 3.4.

Due to the short reaction duration of JHVCTR process, the production rate of magnesium above 200 g·day^{-1} has been realized in the laboratory. Given that the size of CaO·MgO-C pellets can be scaled up to tens of kilograms, the JHVCTR process could hold great promise for high-throughput mass production of magnesium. Additionally, the automated operation achieved by mechanical devices can further improve the output for future production. Notably, the power of the JHVCTR process can be supplied by renewable electricity readily, whereas the reduction of MgO can be driven by renewable energy resources (including solar light, wind, and so on), facilitating the whole process to more environment-friendly and sustainable. Overall, our proposed approach holds massive potential for the practical preparation of magnesium. However, due to the need for a vacuum environment, the continuous operation of the JHVCTR process remains challenging, as with the traditional VCTR process. Therefore, a number of scientific and technological issues still need to be addressed.

3.6. Energy consumption assessment

Additionally, the energy consumption of the JHVCTR process was evaluated (Supplementary Note 1) and compared with the traditional VCTR process. Owing to the in-situ heating nature, rapid heating/cooling rate, volumetric heating feature, and the short reaction times, the JHVCTR process is highly efficient and energy-saving. The energy consumption of the JHVCTR process was estimated to be 5.42 × 10^7 kJ·ton$_{Mg}^{-1}$ (Fig. S5), which is 4.58 % lower than that of the traditional VCTR process (5.68 × 10^7 kJ·ton$_{Mg}^{-1}$) [10]. Therefore, the JHVCTR process for magnesium production could have advantages over the traditional VCTR process.

4. Conclusion

Herein, we developed a JHVCTR process for the preparation of bulk magnesium, which features uniform temperature profiles, rapid heating/cooling, and short reaction times. Firstly, the optimum JHVCTR reaction parameters (input power density and reaction time) were screened, comprehensively taking into account energy and time conservation as well as the high reduction rate. As a result, the reduction rate of MgO of 95.38 % was achieved within 120 s at 0.55 W·mm^{-3}. The kinetic analysis demonstrates that the reaction between MgO and C is dominated by the phase boundary reaction, and the activation energy is 169.1 kJ·mol^{-1}. Based on Joule's law, we proposed a mechanism that Joule heating could form an extremely high-temperature C-MgO interface, which facilitated the processing reactions. Moreover, MD simulations and DFT calculations demonstrated that the applied electric field during the JHVCTR process could reduce the binding ability of MgO, thereby enhancing its reactivity. Furthermore, we studied the condensation behaviors of magnesium vapor at different condensation temperatures. The bulk magnesium with a dense structure and high purity was obtained at 647 °C. Thermodynamic analysis confirmed that high condensation temperatures could mitigate the inverse reaction between magnesium vapor and CO. Finally, the scale-up trials verified the potential feasibility of the JHVCTR process for the industrial production of magnesium. Therefore, we believe that the JHVCTR process proposed could be a promising approach for the rapid and safe preparation of magnesium.

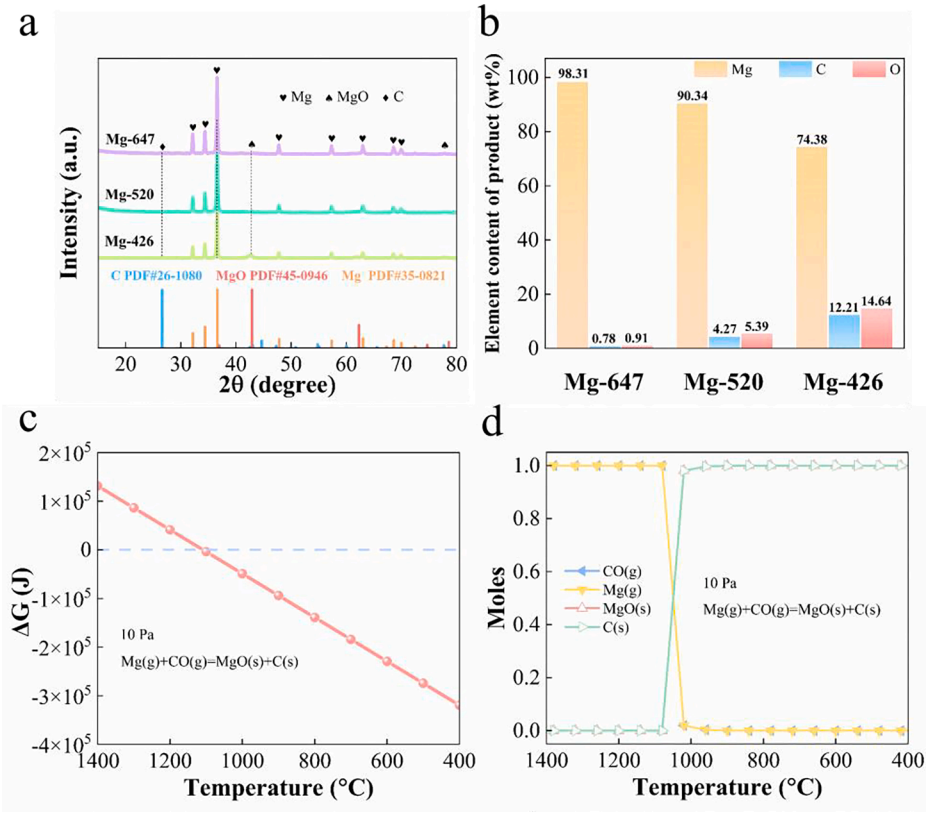

Fig. 12. (a) XRD patterns and (b) quantitative EDS analysis (Mg, C, and O) of Mg-647, Mg-520, and Mg-458. (c) Gibbs free energy (ΔG) calculations and (d) thermodynamic prediction for products of the inverse reaction (Mg + CO = MgO + C) at 10 Pa.

CRediT authorship contribution statement

Xiao Luo: Writing – review & editing, Validation, Software, Methodology, Investigation, Formal analysis, Data curation, Conceptualization. **Peng Zhao:** Visualization, Supervision, Project administration, Funding acquisition. **Jiangjiang Li:** Resources, Methodology.

Declaration of competing interest

The authors declare that they have no known competing financial interests or personal relationships that could have appeared to influence the work reported in this paper.

Acknowledgement

This work was funded by the Natural Scientific Foundation (S2023-JC-YB-0659) of Shaanxi Province.

Appendix A. Supplementary data

Supplementary data to this article can be found online at https://doi.org/10.1016/j.cej.2025.159761.

Data availability

Data will be made available on request.

References

[1] C. Shin, H. Lee, C. Gyan-Barimah, J. Yu, J. Yu, Magnesium: properties and rich chemistry for new material synthesis and energy applications, Chem. Soc. Rev. 52 (6) (2023) 2145–2192, https://doi.org/10.1039/d2cs00810f.
[2] M. Bian, I. Nakatsugawa, Y. Matsuoka, X. Huang, Y. Tsukada, T. Koyama, Y. Chino, Improving the mechanical and corrosion properties of pure magnesium by parts-per-million-level alloying, Acta Mater. 241 (2022) 118393, https://doi.org/10.1016/j.actamat.2022.118393.
[3] M. Danaie, S. Tao, P. Kalisvaart, D. Mitlin, Analysis of deformation twins and the partially dehydrogenated microstructure in nanocrystalline magnesium hydride (MgH_2) powder, Acta Mater. 58 (8) (2010) 3162–3172, https://doi.org/10.1016/j.actamat.2010.01.055.
[4] J. Hirsch, T. Al-Samman, Superior light metals by texture engineering: optimized aluminum and magnesium alloys for automotive applications, Acta Mater. 61 (3) (2013) 818–843, https://doi.org/10.1016/j.actamat.2012.10.044.
[5] S.V.S. Prasad, S.B. Prasad, K. Verma, R.K. Mishra, V. Kumar, S. Singh, The role and significance of magnesium in modern day research – a review, J. Magn. Alloy. 10 (1) (2022) 1–61, https://doi.org/10.1016/j.jma.2021.05.012.
[6] T. Ma, N. Xiong, Y. Tian, G. Zha, B. Yang, B. Xu, L. Wang, D. Liang, H. Yu, Analysis of KF behavior and inverse reaction molecular kinetics simulation in the vacuum carbothermic reduction of magnesium oxide, J. Alloy. Compd. 955 (2023), https://doi.org/10.1016/j.jallcom.2023.170325.
[7] S. Rahimpour Golroudbary, I. Makarava, A. Kraslawski, Environmental assessment of global magnesium production, Miner. Process Extr. Metall. Rev. 44 (6) (2022) 389–406, https://doi.org/10.1080/08827508.2022.2084734.
[8] USGS, MAGNESIUM METAL, (2022). https://doi.org/pubs.usgs.gov/periodicals/mcs2022/mcs2022-magnesium-metal.pdf, 2022 (accessed 1 September 2023).
[9] H. Jeoung, T. Lee, J. Lee, K. Yi, J. Kang, An electrolytic process using an Ag cathode and vacuum distillation for Mg metal production from MgO, J. Sust. Metall. 9 (2) (2023) 688–699, https://doi.org/10.1007/s40831-023-00669-2.
[10] Y. Tian, L. Wang, B. Yang, Y. Dai, B. Xu, F. Wang, N. Xiong, Comparative evaluation of energy and resource consumption for vacuum carbothermal reduction and Pidgeon process used in magnesium production, J. Magn. Alloy. 10 (3) (2022) 697–706, https://doi.org/10.1016/j.jma.2020.09.024.
[11] Y. Tian, B. Xu, B. Yang, C. Yang, T. Qu, D. Liu, Y. Dai, Magnesium production by carbothermic reduction in vacuum, J. Magn. Alloy. 3 (2) (2015) 149–154, https://doi.org/10.1016/j.jma.2015.04.001.
[12] F. Hu, J. Pan, X. Ma, X. Zhang, J. Chen, W. Xie, Preparation of Mg and Ca metal by carbothermic reduction method – a thermodynamics approach, J. Magn. Alloy. 1 (3) (2013) 263–266, https://doi.org/10.1016/j.jma.2013.08.004.
[13] W. Xie, J. Chen, H. Wang, X. Zhang, X. Peng, Y. Yang, Kinetics of magnesium preparation by vacuum-assisted carbothermic reduction method, Rare Met. 35 (2) (2014) 192–197, https://doi.org/10.1007/s12598-014-0275-6.
[14] Y. Jiang, Y. Liu, H. Ma, W. Zhou, Mechanism of calcium fluoride acceleration for vacuum carbothermic reduction of magnesia, Metall. Mater. Trans. B-Proc. Metall. Mater. Proc. Sci. 47 (2) (2015) 837–845, https://doi.org/10.1007/s11663-015-0531-7.
[15] N. Xiong, Y. Tian, X. Chen, K. Li, B. Xu, B. Yang, Y. Dai, Dynamic simulation and experimental study of magnesia formed between magnesium vapor and CO under

vacuum, JOM 71 (8) (2019) 2791–2797, https://doi.org/10.1007/s11837-019-03489-6.
[16] N. Xiong, Y. Tian, B. Yang, B. Xu, D. Liu, Y. Dai, Volatilization and condensation behaviours of Mg under vacuum, Vacuum 156 (2018) 463–468, https://doi.org/10.1016/j.vacuum.2018.08.014.
[17] Y. Tian, B. Xu, C. Yang, B. Yang, T. Qu, H. Liu, Y. Dai, D. Liu, Analysis of magnesia carbothermic reduction process in vacuum, Metall. Mater. Trans. B-Proc. Metall. Mater. Proc. Sci. 45 (5) (2014) 1936–1941, https://doi.org/10.1007/s11663-014-0106-z.
[18] N. Xiong, Y. Tian, B. Yang, B. Xu, T. Dai, Y. Dai, Results of recent investigations of magnesia carbothermal reduction in vacuum, Vacuum 160 (2019) 213–225, https://doi.org/10.1016/j.vacuum.2018.11.007.
[19] B.A. Chubukov, A.W. Palumbo, S.C. Rowe, I. Hischier, A.J. Groehn, A.W. Weimer, Pressure dependent kinetics of magnesium oxide carbothermal reduction, Thermochim. Acta 636 (2016) 23–32, https://doi.org/10.1016/j.tca.2016.03.035.
[20] L. Rongti, P. Wei, M. Sano, Kinetics and mechanism of carbothermic reduction of magnesia, Metall. Mater. Trans. B-Proc. Metall. Mater. Proc. Sci. 34 (4) (2003) 433–437, https://doi.org/10.1007/s11663-003-0069-y.
[21] G. Brooks, S. Trang, P. Witt, M.N.H. Khan, M. Nagle, The carbothermic route to magnesium, JOM 58 (5) (2006) 51–55, https://doi.org/10.1007/s11837-006-0024-x.
[22] A. Koo, G.A. Brooks, M. Nagle, Nucleation and growth of Mg condensate during supersonic gas quenching, J. Cryst. Growth 310 (10) (2008) 2659–2667, https://doi.org/10.1016/j.jcrysgro.2008.01.036.
[23] M. Mittal, Explosion characteristics of micron- and nano-size magnesium powders, J. Loss Prev. Process Ind. 27 (2014) 55–64, https://doi.org/10.1016/j.jlp.2013.11.001.
[24] K.M. Wyss, D.X. Luong, J.M. Tour, Large-scale syntheses of 2D materials: flash joule heating and other methods, Adv. Mater. 34 (8) (2022) 2106970, https://doi.org/10.1002/adma.202106970.
[25] Q. Dong, Y. Yao, S. Cheng, K. Alexopoulos, J. Gao, S. Srinivas, Y. Wang, Y. Pei, C. Zheng, A.H. Brozena, H. Zhao, X. Wang, H.E. Toraman, B. Yang, I.G. Kevrekidis, Y. Ju, D.G. Vlachos, D. Liu, L. Hu, Programmable heating and quenching for efficient thermochemical synthesis, Nature 605 (7910) (2022) 470–476, https://doi.org/10.1038/s41586-022-04568-6.
[26] B. Deng, D.X. Luong, Z. Wang, C. Kittrell, E.A. McHugh, J.M. Tour, Urban mining by flash Joule heating, Nat. Commun. 12 (1) (2021) 5794, https://doi.org/10.1038/s41467-021-26038-9.
[27] B. Deng, W. Meng, P.A. Advincula, L. Eddy, M.G. Ucak-Astarlioglu, K.M. Wyss, W. Chen, R.A. Carter, G. Li, Y. Cheng, S. Nagarajaiah, J.M. Tour, Heavy metal removal from coal fly ash for low carbon footprint cement, Commun. Eng. 2 (1) (2023), https://doi.org/10.1038/s44172-023-00062-7.
[28] B. Deng, S. Xu, L. Eddy, J. Shin, Y. Cheng, C. Kittrell, K. JeBailey, J. Sharp, L. Qian, S. Chen, J.M. Tour, Flash separation of metals by electrothermal chlorination, Nat. Chem. Eng. 1 (10) (2024) 627–637, https://doi.org/10.1038/s44286-024-00125-2.
[29] X. Luo, P. Zhao, J. Guo, J. Li, A rapid and environment-friendly process for dolomite pellets calcination with Joule-heating, J. Clean. Prod. 434 (2024), https://doi.org/10.1016/j.jclepro.2023.140173.
[30] B.A. Chubukov, A.W. Palumbo, S.C. Rowe, M.A. Wallace, K.Y. Sun, A.W. Weimer, Design and fabrication of pellets for magnesium production by carbothermal reduction, Metall. Mater. Trans. B-Proc. Metall. Mater. Proc. Sci. 49 (5) (2018) 2209–2218, https://doi.org/10.1007/s11663-018-1309-5.
[31] M. Broda, A.M. Kierzkowska, C.R. Müller, Development of highly effective CaO-based, MgO-stabilized CO_2 sorbents via a scalable "One-Pot" secrystallization technique, Adv. Funct. Mater. 24 (36) (2014) 5753–5761, https://doi.org/10.1002/adfm.201400862.
[32] J. Puig, M. Balat-Pichelin, Experimental carbothermal reduction of MgO at low pressure using concentrated solar energy, J. Min. Metall. Sect. B-Metall. 54 (1) (2018) 39–50, https://doi.org/10.2298/jmmb170215048p.
[33] I.M. Morsi, H.H. Ali, Kinetics and mechanism of silicothermic reduction process of calcined dolomite in magnetherm reactor, Int. J. Miner. Process. 127 (2014) 37–43, https://doi.org/10.1016/j.minpro.2013.11.016.
[34] W. Chen, J. Chen, K.V. Bets, R.V. Salvatierra, K.M. Wyss, G. Gao, C.H. Choi, B. Deng, X. Wang, J. Li, C. Kittrell, N. La, L. Eddy, P. Scotland, Y. Cheng, S. Xu, B. Li, M.B. Tomson, Y. Han, B.I. Yakobson, J.M. Tour, Battery metal recycling by flash Joule heating, Sci. Adv. 9 (39) (2023), https://doi.org/10.1126/sciadv.adh5131.
[35] B. Deng, P.A. Advincula, D.X. Luong, J. Zhou, B. Zhang, Z. Wang, E.A. McHugh, J. Chen, R.A. Carter, C. Kittrell, J. Lou, Y. Zhao, B.I. Yakobson, Y. Zhao, J.M. Tour, High-surface-area corundum nanoparticles by resistive hotspot-induced phase transformation, Nat. Commun. 13 (1) (2022), https://doi.org/10.1038/s41467-022-32622-4.
[36] Z. Huang, Y. Yao, Z. Pang, Y. Yuan, T. Li, K. He, X. Hu, J. Cheng, W. Yao, Y. Liu, A. Nie, S. Sharifi-Asl, M. Cheng, B. Song, K. Amine, J. Lu, T. Li, L. Hu, R. Shahbazian-Yassar, Direct observation of the formation and stabilization of metallic nanoparticles on carbon supports, Nat. Commun. 11 (1) (2020) 6373, https://doi.org/10.1038/s41467-020-20084-5.
[37] Z. Song, C. Liang, K. Gong, S. Zhao, X. Yuan, X. Zhang, J. Xie, Harnessing the high interfacial electric fields on water microdroplets to accelerate menshutkin reactions, J. Am. Chem. Soc. 145 (48) (2023) 26003–26008, https://doi.org/10.1021/jacs.3c11650.
[38] K.C. Hass, W.F. Schneider, A. Curioni, W. Andreoni, The chemistry of water on alumina surfaces: reaction dynamics from first principles, Science 282 (5387) (1998) 265–268, https://doi.org/10.1126/science.282.5387.265.
[39] J. Narayan, Unified model of field assisted sintering and related phenomena, Scr. Mater. 176 (2020) 117–121, https://doi.org/10.1016/j.scriptamat.2019.09.012.
[40] D. Liang, L. Wang, Y. Tian, B. Yang, B. Xu, W. Zhao, T. Ma, Preparation of high purity magnesium by vacuum gasification-directional condensation technology, Sep. Purif. Technol. 327 (2023), https://doi.org/10.1016/j.seppur.2023.124878.
[41] J. Han, D. Fu, J. Guo, Z. Ji, Z. Dou, T.a. Zhang, Nucleation and condensation of magnesium vapor in argon carrier, Metals 10 (11) (2020), https://doi.org/10.3390/met10111441.
[42] C. Yang, Y. Tian, T. Qu, B. Yang, B. Xu, Y. Dai, Magnesium vapor nucleation in phase transitions and condensation under vacuum conditions, Trans. Nonferrous Met. Soc. China 24 (2) (2014) 561–569, https://doi.org/10.1016/s1003-6326(14)63096-x.